Unsteady two-dimensional orifice flow: a large-size experimental investigation

Ecoulement non-permanent dans un orifice rectangulaire: une étude experimentale de grande taille

Hubert CHANSON, MIAHR, *Reader, Fluid Mechanics, Hydraulics and Environmental Engineering, Department of Civil Engineering, The University of Queensland, Brisbane QLD 4072, Australia (e-mail: h.chanson@mailbox.uq.edu.au)*

Shin-ichi AOKI, and Mamoru MARUYAMA, *Department of Architecture and Civil Engineering, Toyohashi University of Technology, Toyohashi 441-8580, Japan (e-mail: aoki@jughead.tutrp.tut.ac.jp)*

ABSTRACT
Orifice flows were used as water clocks since the Antiquity up to the 16-th century. Today orifices and nozzles are used for measuring discharges. Most works were conducted with steady flow conditions and there is little information on the unsteady flow pattern. In this study, the writers describe an experimental investigation of an unsteady orifice flow discharging vertically. The study was conducted in a large-size facility with a rectangular orifice (0.75-m by 0.07-m) discharging up to 1.2 m^3 in about 10 seconds. The study presents new information on the unsteady flow patterns, the discharge capacity and the velocity field in the reservoir. The results are compared with ''classical'' orifice flow results.

RÉSUMÉ
Les écoulements dans les orifices ont été utilises comme horloges à eau depuis l'Antiquité jusqu'au $16^{ième}$ siècle. De nos jours les orifices et les ajutages sont utilisés pour les mesures de débit. La plupart des travaux ont été menés en écoulement permanent et l'on manque d'information sur les configurations non permanentes. Dans cet article, les auteurs décrivent l'étude expérimentale d'un écoulement instationnaire débitant verticalement par un orifice. Les essais ont été faits dans une installation de grande taille avec un orifice rectangulaire (0.75 m sur 0.07 m), évacuant jusqu'à 1.2 m^3 en 10 secondes environ. L'étude présente des informations nouvelles sur les configurations de l'écoulement instationnaire, la coefficient de débit et le champ de vitesse dans le réservoir. Les résultats sont comparés avec les résultats ''classiques'' des écoulements dans les orifices.

Introduction

Orifice flows were used as water clock (i.e. clepsydra) in ancient Babylon and Egypt as well as in parts of Africa and by some North America Indians. (Hero of Alexandria wrote a treaty on water clocks in four books.) They were in use up to the 16-th century. Today the sand glass uses the same principle with granular material. Orifices and nozzles are used also for measuring discharges. In his study of orifice flows, J.C. de BORDA (1733-1799) made a significant contribution by not only introducing the concept of streamlines but also by developing the "Borda" mouthpiece to measure accurately the orifice flow.

When water flow through a sharp-edged orifice, the jet flow contracts to have its smallest section a small distance downstream of the hole. For a horizontal jet, Bernoulli principle implies that the velocity at vena contracta equals $\sqrt{2*g*H}$ where H is the reservoir head above orifice centreline. (This relationship is called Torricelli theorem, after Evangelista TORRICELLI (1608-1647).) By continuity, the orifice discharge equals:

$$Q = C_D * A_o * \sqrt{2 * g * H} \quad (1)$$

where A_o is the orifice cross-section area. The discharge coefficient C_D may be expressed as:

$$C_D = C_c * C_V \quad (2)$$

where the velocity coefficient C_v account for the energy losses and the contraction coefficient C_c equals A/A_o, A being the jet cross-section area at vena contracta. For a horizontal water jet discharging from an infinite reservoir, C_c equals 0.58 and 0.61 for axisymmetrical and two-dimensional jets respectively (HUNT 1968, JOUKOWSKI 1890, MICHELL 1890, MISES 1917). The value of C_c increases with increasing relative nozzle area when the reservoir is of finite dimensions.

Most works were conducted with steady flow conditions and there is little information on the unsteady flow properties. In this paper, the writers describe an experimental investigation of an unsteady orifice flow. The study was conducted in a large-size facility with a rectangular orifice (0.75-m by 0.07-m) discharging vertically up to 1.2 m^3 in about 10 seconds. The study is focused on the unsteady flow patterns, the discharge capacity and the velocity field in the reservoir. The results are compared with classical results. It is the purpose of this paper to assess critically the overall state of this topic and to present new compelling conclusions valid for two-dimensional orifice flows discharging vertically.

Experimental configuration

New experiments were performed with a rectangular sharp-edge orifice (0.750-m by 0.070-m) made from a 10-mm thick perspex sheet and located at the bottom of a circular water tank, 0.8-m high with internal diameter ranging from 1.3 m at the base up to 1.35-m at the top (Fig. 1). The orifice dimensions were selected to minimise scale-effects associated with small-size orifices, and

Revision received November 16, 2000. Open for discussion till August 31, 2002.

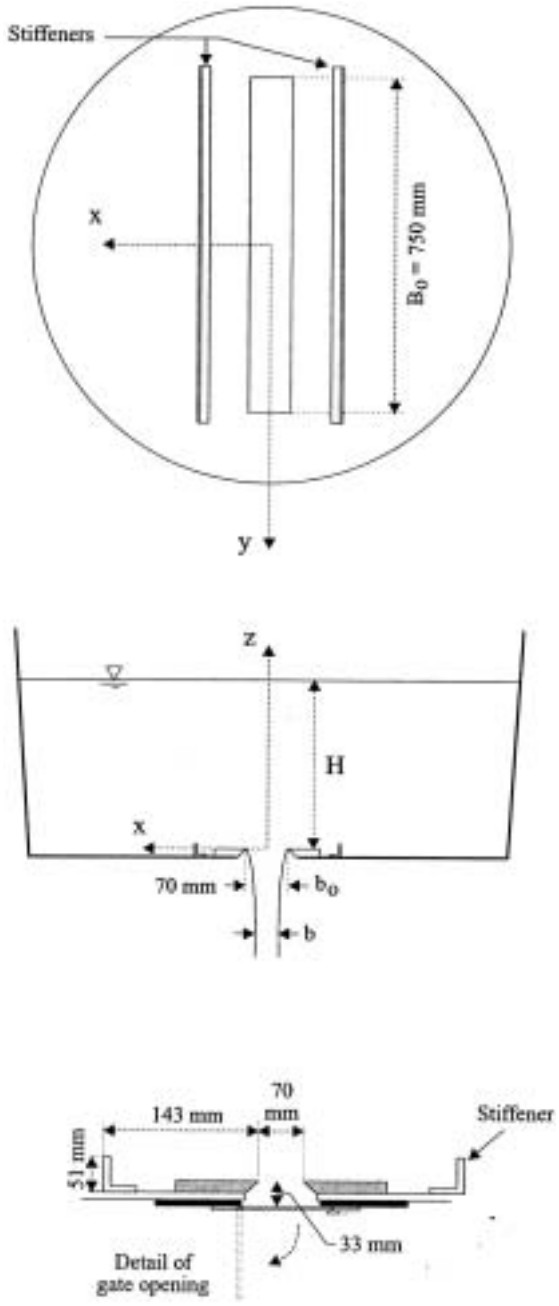

Fig. 1 Sketch of the experiment and definition sketch

the ratio of width to thickness was chosen to achieve a quasi-two-dimensional flow. The orifice was closed by a 4.1-kg steel gate (0.11 m × 0.79 m × 0.006 m). Two L-shaped stiffners were added inside the tank and located parallel to the orifice. Their upper edge was 41-mm above the orifice and they were placed 143-mm apart from the orifice centreline. Flow visualisations suggested that the stiffeners had little effect on the orifice flow for head above orifice larger than 0.1-m.

The relationship between the water elevation above orifice edge and water volume was measured in-situ with a calibrated 40-L container :

$$\text{Volume} = 1.3889 * (H + 0.01)^{1.035455} \quad 0 \le H \le 0.8 \text{ m} \quad (3)$$

where H is the total head above orifice edge, with a normalised correlation coefficient of 0.999989. During the experiments, the orifice flow discharged vertically into a large container located at least 1.5-m beneath the orifice. Further experimental details were reported in CHANSON et al. (2000).

Time origin and system of references

Gate opening resulted from unlatching three pins with a hammer. High-speed video pictures demonstrated that the unlatching occurred in less than 30 milliseconds and the full opening of the gate took about 180 to 230 milliseconds. The time origin (t=0) is taken at the time of impact of the hammer on the pins. The origin of the system of coordinates {x, y, z} is taken at the centre of the orifice with z positive upwards, x along the short orifice centreline and y along the long centreline (Fig. 1).

Instrumentation

Flow visualisations and nappe trajectory were investigated with two video-cameras : a VHS-C camescope National™ CCD AG-30C (speed: 30 frames/sec., shutter: 1/60 & 1/1,000 sec.) and a digital handycam Sony™ DV-CCD DCR-TRV900 (speed: 30 frames/sec., shutter: 1/4 to 1/10,000 sec., zoom: 1 to 48).

Water depths in the tank were measured with pointer gauges and a 0.8-m long capacitance wave gauge. The wave gauge has a 10-Hz response and an accuracy of about 1-mm that was tested during on-site calibration with the pointer gauges. It was calibrated daily by comparing the voltage output with point gauge readings for a range of water heights, and calibration curves were best-fitted to the readings.

Velocity measurements were performed with a 3-D acoustic Doppler velocimeter (ADV) Nortek™ ADVLab equipped with a downlooking sensor mounted on a rigid 40-cm stem. (On-site measurements showed that the distance from the sampling volume to the probe tip was 55-mm.) The system was calibrated in factory and it should not need re-calibration. The accuracy on the velocity was expected to be about 0.025 m/s (Nortek 1996) but larger errors were experienced close to the orifice because of the size of the sampling volume. The latter was approximately 6-mm in diameter (Nortek 1996). The accuracy of the ADV velocity was supposed to equal the velocity difference across the sampling volume.

The ADV system was oriented in the yz-plane with a 40- to 60-degrees angle to the horizontal to avoid wake interference caused by the probe tip into the sampling volume. (Flow visualisations confirmed the absence of interference from the probe transducers on the sampling volume.) The three velocity components were reconstructed by a rotation around the Ox axis.

ADV-velocity data noise

High levels of noise were observed in the three velocity component signals. At rest the measured ADV signal represents the Doppler noise itself. Once the orifice gate was opened, the observed velocity fluctuations characterised the combined effects of the Doppler noise, velocity fluctuations and installation vibra-

tions. It is acknowledged that the Doppler noise level increases with increasing velocity although it remains of the same order of magnitude as the Doppler noise at rest : e.g., NIKORA and GORING (1998) and more specifically LEMMIN and LHERMITTE (1999).
No turbulence measurement could be performed accurately during the study because the Doppler noise was of the same order of magnitude as (if not larger than) true turbulent velocity fluctuations.

Experimental results. (1) Unsteady flow patterns

The unsteady flow pattern resulting from the gate opening is characterised by an initial phase with rapid aeration of the water next to the orifice (mixing flow), a flow acceleration phase associated with free-jet expansion downstream of the orifice (bursting flow), a quasi-steady flow period and, near the end, a free-surface flow over the orifice edges (Table 1, Fig. 2 and 3). Overall the discharge duration was about 10 seconds for an initial water volume of one thousand litres. Photographs of the orifice flow are shown in Figure 3.

Table 1 Unsteady orifice flow patterns

t	Flow pattern
(1)	(2)
$0 \Rightarrow$ 68 to 133 ms	Mixing flow
67 to 133 ms $\Rightarrow$ 150 to 230 ms	Bursting flow
150 to 230 ms $\Rightarrow$ H/b_o>0,5	Quasi-steady flow
H/b_o<0.43 to 0.5	Free-surface flow (weir overflow)

Notes: b_o : short orifice dimension; H : head above orifice (Fig. 1 and 2).

Mixing flow / Multiphase flow

In the initial instants following the gate unlatching, the hydrostatic pressure force acting on the gate adds to the weight of the gate and contributes to a rapid gate opening. However the jet flow starts slowly and accelerates with time t.
Visual observations with an underwater camera located inside the reservoir showed that some air tends to flow upwards into the reservoir up to and slightly above the orifice edge for t > 0. The duration of this mixing phase is about 67 to 133 ms (2/30 to 4/30 s). The air bubbles are observed to enter all around the gate, although the bubbly flow region is not two-dimensional (Fig. 2). Little air is observed near the orifice centreline (i.e. y = 0). The maximum elevation reached by the air was about 5 to 10 mm above orifice edge. Afterwards the air was entrained downwards by the jet flow. The flow pattern was observed consistently for $0.3 < H_1 < 0.75$ m and t < 67 to 133 ms.

Remark

The gate opening is somewhat analogous to a negative surge at a penstock forebay (e.g. HENDERSON 1966, pp. 322-324; MONTES 1998, pp. 487-489). The disturbance (i.e. negative wave) propagates with a speed $C = \sqrt{g*H_1}$. (In a particular case, experimental observations showed that the celerity of the negative surge was $2*\sqrt{g*H_1}$ (LAUBER and HAGER 1998).) By analogy, the disturbance created by the sudden orifice opening would reach the free-surface at $t = H_1/C = 257$ ms for $H_1 = 0.65$ m : i.e., a time scale similar to the duration of the mixing flow.
Another analogy would be the water hammer. The circular tank is somehow analogous to a 1.3-m diameter fibreglass pipe in which the wave celerity is about C ~ 300 m/s. The time period of pressure oscillations in the tank is $4*H_1/C = 8.7$ ms for $H_1 = 0.65$ m. Such a time frame is one to two orders of magnitude smaller than the duration of the mixing flow.

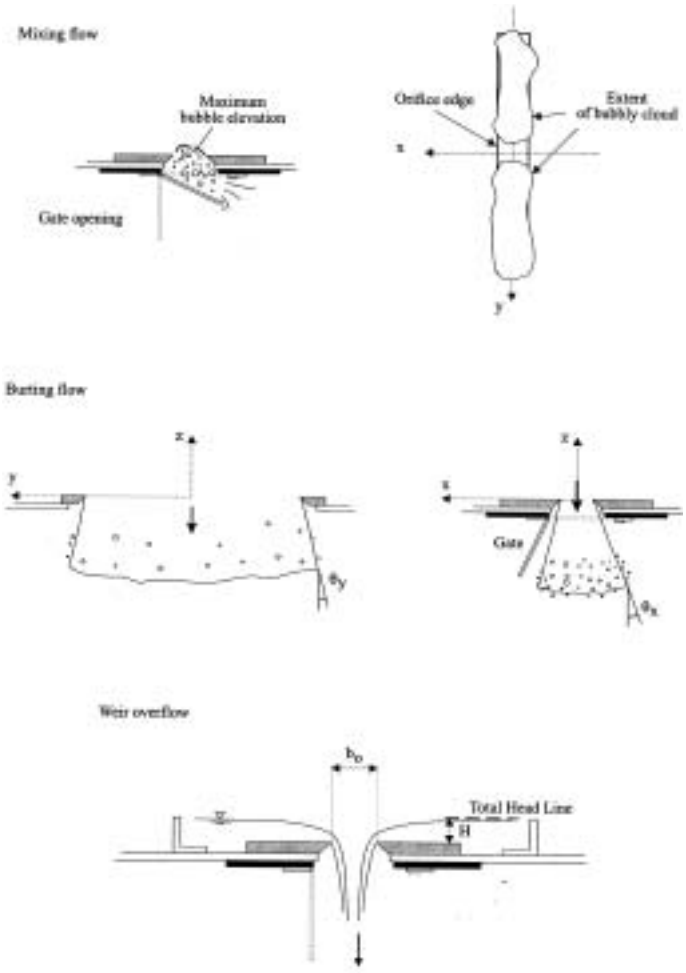

Fig. 2 Sketch of the basic orifice flow sequences

Bursting jet / Accelerating flow

Once the reservoir water accelerate, the jet flow bursts downwards out of the orifice (Fig. 2 and 3). The leading edge of the jet is preceded by aerated waters spreading in both the x- and y-directions (i.e. "bursting flow"). Experimental observations indicate that the lateral spread angles of the jet θ_x and θ_y are nearly independent of the initial total head : i.e., $\theta_x = 33$ to 55° and $\theta_y \sim 15°$ for $0.3 < H_1 < 0.75$ m. The "bursting flow" lasts about 150 to 230 ms at the orifice.
It was initially thought that the "bursting flow" was caused by the

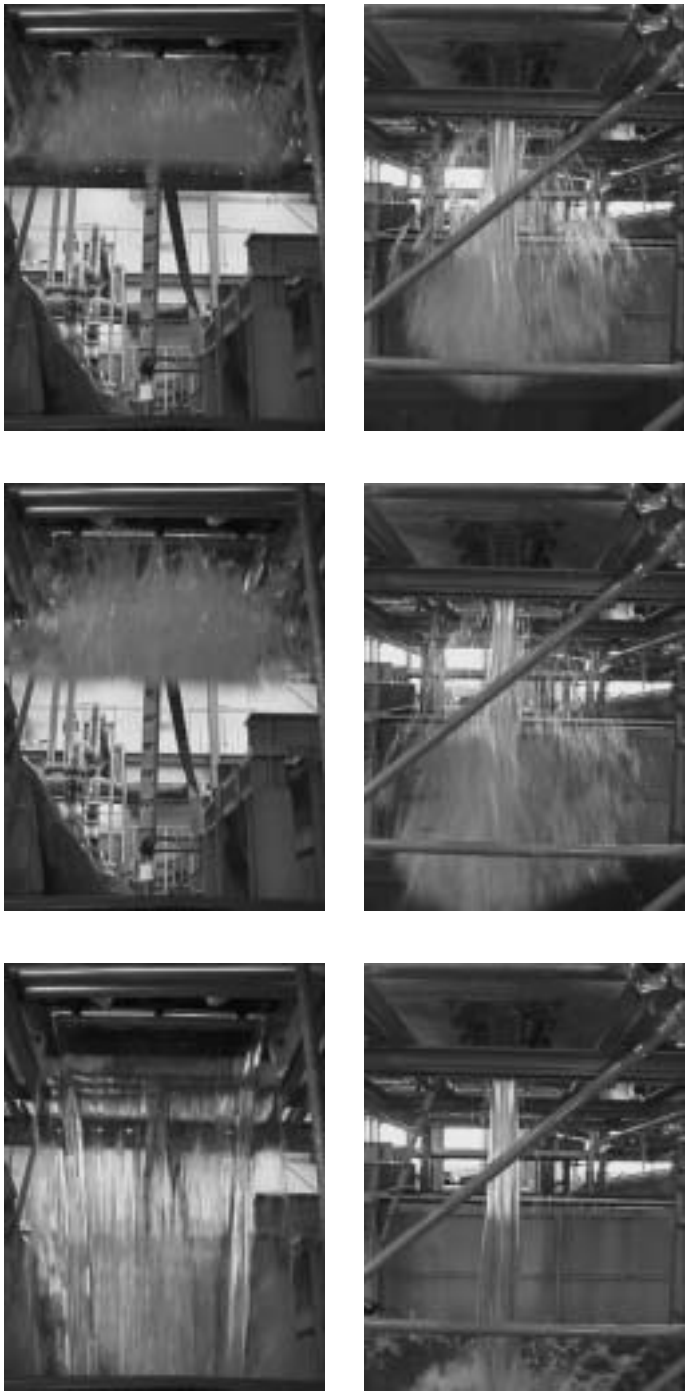

Fig. 3 Photographs of an experiment (H_1 = 0.652 m)

Left Front view	Right Sideview
(a1) Initial bursting flow	(a2) Bursting flow
(b1) Bursting flow	(b2) End of bursting flow
(c1) Quasi-steady flow	(c2) Quasi-steady flow

sudden expansion of the water volume located between the gate and the orifice (i.e. - 33 mm < z < 0) (Fig. 1, bottom). The writers believe that the flow pattern results instead from the sudden expansion of the air-water mixture generated during the initial instants (i.e. mixing flow phase).

Note that, for very-small circular jets (millimetric size) discharging vertically from a cylinder, the leading edge of the jet was observed to have a round bulging shape (STORR and BEHNIA 1999). It is likely that surface tension prevented the aeration of the jet edges during these experiments.

Quasi-steady flow

After the establishment of the jet flow, the flow pattern becomes quasi-steady. Nappe contraction is observed downstream of the orifice (Fig. 3). The observed nappe contraction b/b_o is best correlated by :

$$\frac{b}{b_0} = 0.94 - 0.021 * \frac{H_1}{b_0} \quad \text{for} \quad 5 < H/b_o < 11 \tag{4}$$

where b is the free-falling nappe thickness observed at $z/b_o \sim -1$. The nappe contraction in the y-direction was observed to be: $B/B_o \approx 0.8$ to 0.85. In comparison, for rectangular sharp-crested weirs with side contractions, the lateral contraction of the overflow nappe is about 0.8 (e.g. ACKERS et al. 1978, pp. 59-61).

Dye injection in the tank associated with underwater video-pictures confirmed the smooth flow contraction into the orifice. No dye mixing was observed anywhere anytime in the reservoir. The observation was valid everywhere including around the ADV sensors.

Free-surface overflow / weir overflow

Near the end of each experiment, the orifice becomes a weir. That is, the flow changes from a submerged flow to a free-surface overflow (Fig. 2). Video observations suggest that the orifice flow becomes a free-surface flow for $H/b_o \approx 0.43$ to 0.51.

Experimental results. (2) Orifice discharge coefficient

For a horizontal jet discharging through a two-dimensional orifice, the flow rate equals:

$$Q = C_D * B_o * b_o * \sqrt{2 * g * H} \tag{1a}$$

where B_o and b_o are the orifice dimensions and C_D is a discharge coefficient that takes into account the nappe contraction downstream of the orifice and the energy losses. Assuming that the reservoir free-surface area *A* is far greater than the orifice area (i.e. $A >> B_o * b_o$), the reservoir surface drops slowly enough and the Bernoulli principle (i.e. Eq. (1)) may be applied with a small error. The continuity equation for an incompressible fluid states that the outflow equals the change of reservoir volume :

$$Q * \Delta t = - A * \Delta H \tag{5}$$

where Δt is a small time interval. Combining Equations (1) and (5), and integrating between $H = H_1$ at $t = t_1$ and $H = H_2$ at $t = t_2$, it yields :

$$t_2 - t_1 = \frac{-1}{\sqrt{2*g} * B_0 * b_0} * \int_{H_1}^{H_2} \frac{A}{C_D * \sqrt{H}} * dH \tag{6}$$

A further assumption is that C_D is nearly constant :

$$t_2 - t_1 = \frac{-1}{\sqrt{2*g}*C_D*B_0*b_0} * \int_{H_1}^{H_2} \frac{A}{\sqrt{H}} * dH \qquad (7)$$

During the present series of experiments, C_D was found to be independent of time (i.e. constant for a given experiment) provided that H > 0.1 to 0.15 m. The discharge coefficient C_D was found to be between 0.62 and 0.65 (Fig. 4, appendix). These values are larger than those predicted by ideal-fluid flow theory and data for orifice flow discharging horizontally : $C_D = 0.60$ (e.g. TROSKOLANSKI 1960).

For an orifice flow discharging vertically, the fluid is accelerated between the orifice and the vena contracta. Equation (7) does not account for the difference in elevation between the orifice and the vena contracta. Video pictures suggest that a "pseudo-vena contracta" occurs at about $z \approx -1.0*b_o$. The observation is subjective as the fluid is accelerated. (For a horizontal two-dimensional orifice, the vena contracta is observed about 1.7 times the orifice height downstream of the orifice (e.g. MONTES 1998, pp. 283-284).). Equations (1) and (7) may be corrected accordingly:

$$Q = C_D' * B_O * b_O * \sqrt{2 * g * (H + 1.0*b_O)} \qquad (1b)$$

$$t_2 - t_1 = \frac{-1}{\sqrt{2*g}*C_D*B_0*b_0} * \int_{H_1}^{H_2} \frac{A}{\sqrt{H+1.0*b_0}} * dH \qquad (7b)$$

Using Equation (7b), the corrected discharge coefficient C_D' was found to be correlated to the initial head above orifice as :

$$C_D = 0.5832 * \left(1 - \exp\left(-0.6597 * \frac{H_1}{b_0}\right)\right) \qquad (8)$$

where H_1 is the initial upstream head above orifice and b_o is the orifice width. The results are presented in Figure 4. They are consistent with the observed nappe contraction (i.e. $b/b_o \approx 0.7$ to 0.85, $B/B_o \approx 0.8$ to 0.85) implying an average contraction coefficient of about $C_c = A/A_o \approx 0.60$. For large head above orifice, the data yield $C_D' \approx 0.58$, a result close to ideal fluid flow results (i.e. C_c = 0.61, MISES 1917). In Figure 4, the results for low ratios H_1/b_o (i.e. less than 4.5) must be considered with due care. First the duration of the jet flow is short before the appearance of a free-surface flow (or weir overflow), and the data accuracy is average. Secondly the assumption of a "pseudo-vena contracta" at $z \approx -1.0*b_o$ might be untrue. For a horizontal sluice gate, it is acknowledged that the flow is unstable when $H_1/b_o < 4$ where the sluice gate opening is $b_o/2$ (e.g. MONTES 1997,1998).

For completeness, the writers wish to highlight the sensitivity of C_D' to the vertical location of the pseudo-vena contracta. Although the present selection ($z/b_o = -1$) is subjective, the results are consistent with independent visual observations of the nappe contraction.

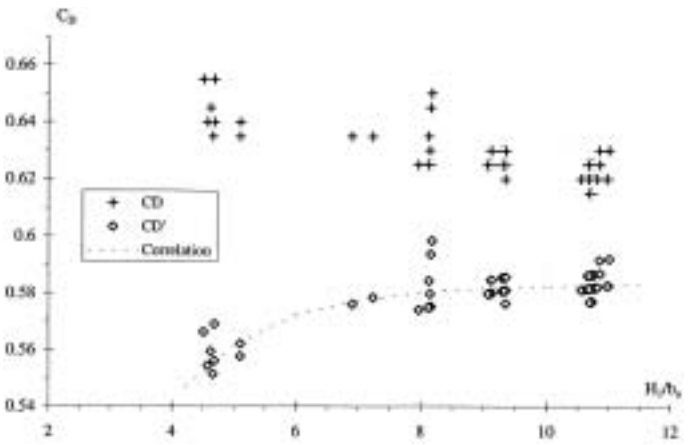

Fig. 4 Orifice discharge coefficient: experimental data

Discussion : modification of the orifice shape

For one series of experiments, the orifice geometry was modified by inserting some 18-µm thick cellophane sheets between the stiffener edges and the orifice (Fig. 5). The cellophane sheets were added to minimise the possible effects during the bursting flow and the spreading of the leading edge of the jet.

The cellophane sheets were clipped onto the stiffeners with a smooth rounded cover. The sheets were slightly wider than the orifice width ($B_o = 0.75$ m) and they extended up to 2-m below the orifice. Video-pictures showed that the plastic cellophanes were stretched between the stiffeners and the orifice edges and they adhered to the jet interfaces without affecting visually the jet flow, but very close to the outer edges of the free-jet.

Experimental results expressed either in terms C_D (Eq. (1)) or C_D' (Eq. (1b)) showed that the discharge coefficients increased by 20 to 25% typically. The increase of discharge capacity is best correlated by:

$$C_D = 0.6734 + 0.0083 * \frac{H_1}{b_0} \qquad \text{with plastic film} \qquad (9)$$

It is believed that the plastic sheets induced three effects : a convergence ($\delta = 16°$) into the orifice, a smoother wall roughness upstream of the orifice edges, and a "smooth-rounding" of the orifice edges. Several researchers showed that a convergence of the reservoir boundaries increases the discharge coefficient of an orifice (Table 2). For irrotational motion of ideal fluid, the contraction coefficient C_c rises from 0.61 to 0.65 for $\delta = 0°$ and 16° respectively assuming zero gravity and for an infinite reservoir (e.g. MONTES 1997). The plastic cellophane sheets created further smooth convergent walls. It is expected that lesser energy losses and hence a greater velocity coefficient C_v would occur.

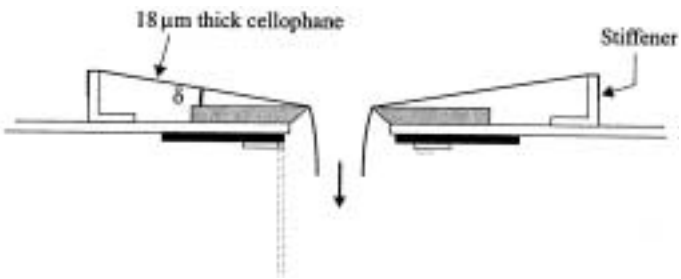

Fig. 5 Modification of the orifice geometry with thin plastic sheets

Table 2 Effect of convergent on contraction coefficient

Reference (1)	Formulation (2)	Remarks (3)
Irrotational motion of ideal fluid		
VALLENTINE (1969)	$C_D = \frac{\pi}{\pi+2}$ for $\delta = 0$ for $\delta = 0$	Two-dimensional orifice flow. Ideal-fluid flow theory. Infinite volume.
	$C_D = \frac{\pi}{\pi+1.064}$ for $\delta = 45°$ for $\delta = 45°$	
MONTES (1997) (*)	$C_C = 0.61$ for $\delta = 0$ $C_C = 0.69$ for $\delta = 30°$ $C_C = 0.747$ for $\delta = 45°$	Two-dimensional planar gate. Ideal-fluid flow theory. Infinite volume. Numerical integration, inverse method.
	$C_D = \frac{\pi}{\pi + 2*\int_0^1 \frac{1}{t}*\sin\left(\frac{\pi/2-\delta}{\pi/2}*\sin^{-1} t\right)*dt}$ (*)	Analytical solution for infinite volume. δ in radians.
	$C_C=0.611+0.132*\delta+0.0291*\delta^2+0.0283*\delta^3$ $0 \le \delta \le 90°$ (*)	Correlation (best fit). δ in radians.
Planar gates (sluices)		
HENDERSON (1966)	$C_C=1 - 0.75*(1-\delta/(\pi/2)) + 0.36*(1-\delta/(\pi/2))^2$ for $0 < \delta < 90°$	Horizontal sluice gates. δ in radians.
MONTES (1998)	$C_C=0.46+0.54*\exp.(-0.8*(\pi/2-\delta))$	Horizontal sluice gates. Analysis of experimental results by COZZO. δ in radians.

Notes: C_c : contraction coefficient; C_D : discharge coefficient; (*): re-analysis and correction by the first writer.

Altogether these combined effects does not explain entirely the increase in discharge coefficient. It is proposed that the plastic cellophanes induced a smooth rounding of the orifice edge which in turn generated a form of Coanda effect leading to a thicker free-jet. That is, the flow streamlines would tend to follow the plastic sheet curvature and a smaller contraction coefficient would be observed. Visual observations from both inside the reservoir and below the orifice suggested a lesser streamline contraction associated with some flow attachment to the plastic cellophanes.

Note that, during the experiments, the plastic cellophanes had no effect on the air resistance in the near flow region., but it is acknowledged that long plastic cellophanes would affect air resistance for long free jets.

Experimental results. (3) Velocity field

Detailed velocity measurements were performed in the reservoir upstream of the orifice. Typical data are shown in Figure 6. The data are presented as $V/\sqrt{2*g*H_1}$ versus H/H_1, where V is the velocity component (V_x or V_z), $\sqrt{2*g*H_1}$ is the maximum ideal-flow velocity at the orifice, H is the instantaneous total head above orifice and H_1 is the initial total head (i.e. $H_1 = H(t=0)$). Each curve corresponds to a fixed sampling volume (i.e. x/b_o and z/b_o constant). The data were recorded on the short orifice centreline (i.e. $y \approx 0$).

Figure 6(A) shows the vertical velocity component data V_z measured on the orifice centreline ($x = 0$). The measured free-surface velocity is also shown. Firstly note the scatter of the data that is characteristics of the ADV noise (see above). Secondly the results show some fluid acceleration next to and upstream of the orifice : i.e., for $z/b_o < 3.5$. Above the water velocity is basically equal to the free-surface velocity. Close to the orifice, the velocity magnitude decreases with decreasing total head : i.e., for $1 < z/b_o < 3.5$.

Figure 6(B) presents experimental data recorded above the orifice edge (i.e. $x/b_o = 0.5$). The graph shows smoothed data (using a box technique) with the same legend for the right and left figures. The vertical velocity component data have the same trend as on the centreline ($x=0$) (Fig. 6(B) right). There is however a horizontal velocity component which becomes significant for $z/b_o < 2$ (Fig. 6(A) left).

Figure 6(C) shows measurements performed away from the orifice (i.e. $x/b_o = 3.6$). The (smoothed data) results show that, for decreasing vertical elevation above orifice, the V_x velocity component increases while the V_z component decreases. The trend is consistent with the change in streamline direction (e.g. Fig. 7).

Overall the results are in agreement with irrotational flow analysis. Figure 7 presents a two-dimensional flow net analysis for $H/b_o = 10$. (Close to the orifice, several equipotential lines were not drawn for clarity.)

Conclusion

The present study presents the unsteady pattern of a rectangular orifice flow discharging vertically. The experimental investigation was conducted in a large-size facility with a rectangular orifice (0.75-m by 0.07-m). The orifice flow discharged vertically up to 1.2 m^3 in about 10 seconds.

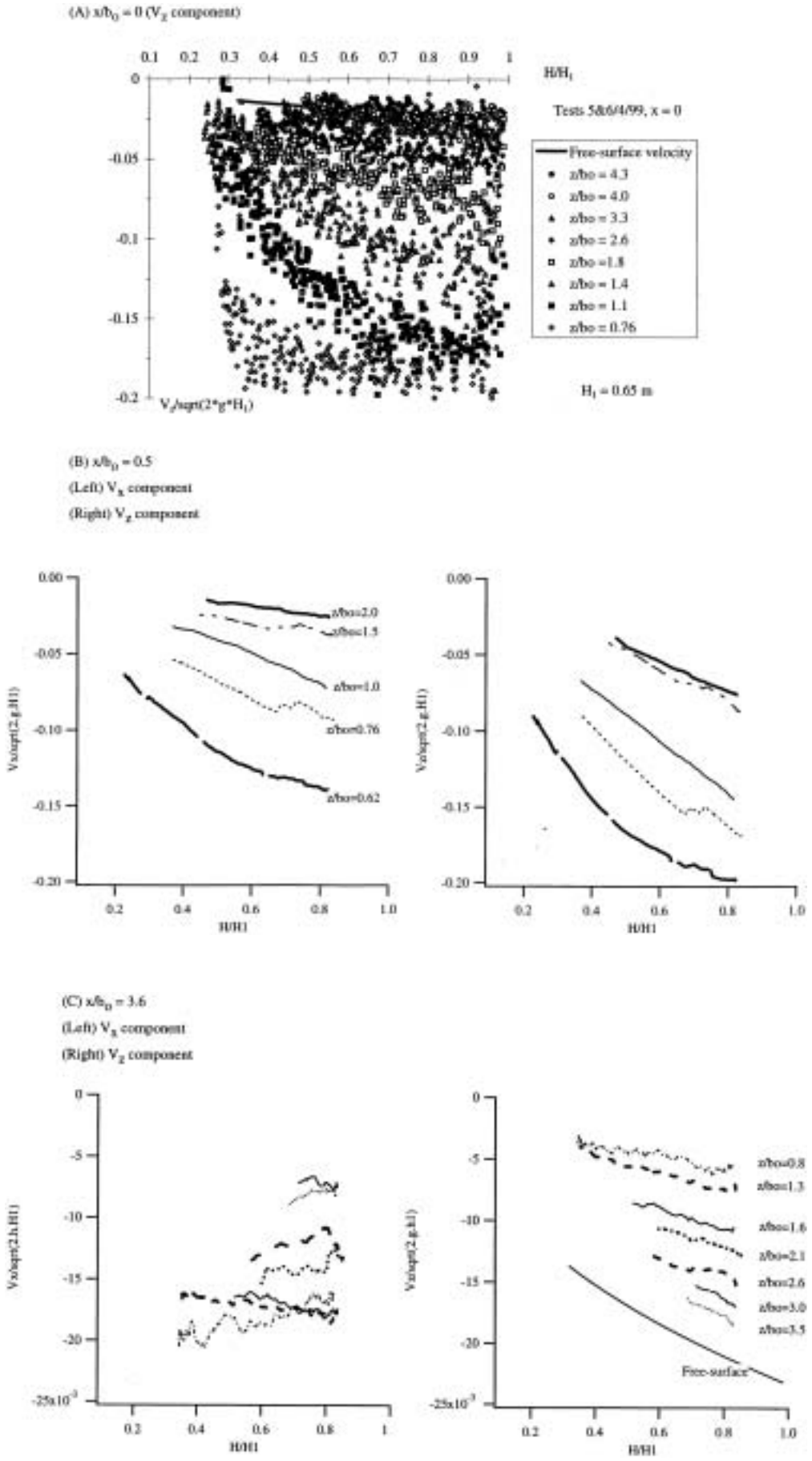

Fig. 6 Unsteady velocity field in the reservoir (b_o = 0.070 m)

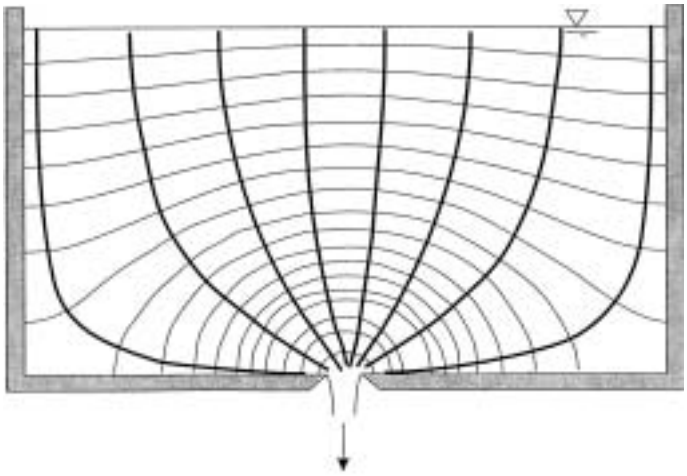

Fig. 7 Two-dimensional flow net analysis ($H/b_o = 10$)

The results highlight four successive flow patterns (Table 1). The gate opening is characterised by an initial phase with rapid aeration of the water next to the orifice (mixing flow), followed by the flow acceleration and free-jet expansion downstream of the orifice (bursting flow), a quasi-steady flow period and, near the end, a free-surface overflow.

The quantitative characteristics of each phase were developed. The discharge coefficient of the vertical orifice flow was found to be very close to that of horizontal orifice flows, although a correction had to account for the vertical jet geometry (Eq. (1b)). The results are consistent with the observations of jet width and thickness. Larger discharge coefficient results were obtained with a converging orifice. The unsteady velocity field is consistent with potential flow calculations. Some fluid acceleration is observed next to and upstream of the orifice (i.e. for $z/b_o < 3.5$) while elsewhere the vertical velocity nearly equals the free-surface velocity. The good agreement between experimental data and ideal-fluid flow theory suggests that boundary effects are small and that the shape of the orifice has little effect provided that the ratio of width to thickness is greater than 10.

In practice, the study provides a newer discharge coefficient correlation for two-dimensional vertical jets, and the result is basically free of scale of effects. Further the experimental results showed that the flow upstream of the orifice is basically an ideal-fluid flow but for the short instants following the gate opening. It was also shown that a sudden orifice gate opening is associated with complex two-phase flow patterns and significant splashing. Further investigations are required to gain a better understanding of the velocity field in the initial phases (mixing and bursting flow). High-speed data acquisition coupled to a high-speed resolution velocitymeter would be needed.

Acknowledgments

The authors acknowledge the support of Professor S. NAKAMURA, Department of Architecture and Civil Engineering, Toyohashi University of Technology (Japan), and the helpful comments of Dr J.S. MONTES, University of Tasmania (Australia). During the first part of the project, the first author was supported by a bilateral fellowship sponsored by the Japan Society of the Promotion of Science and the Australian Academy of Science.

References/bibliographie

ACKERS, P., WHITE, W.R., PERKINS, J.A., and HARRISON, A.J.M. (1978). 'Weirs and Flumes for Flow Measurement.' *John Wiley*, Chichester, UK, 327 pages.

CHANSON, H., AOKI, S., and MARUYAMA, M. (2000). 'Unsteady Two-Dimensional Orifice Flow: an Experimental Study.' *Coastal/Ocean Engineering Report*, No. COE00-1, Dept. of Architecture and Civil Eng., Toyohashi University of Technology, Japan, 29 pages.

HENDERSON, F.M. (1966). 'Open Channel Flow.' *MacMillan Company*, New York, USA.

HUNT, B. (1968). 'Numerical Solution of an Integral Equation for Flow from a Circular Orifice.' *Jl of Fluid Mech.*, Vol. 31, Part 2, pp. 361-177.

JOUKOWSKI, N.E. (1890). 'Modification of Kirchoff's Method for Determining the Two Dimensional Motion of a Fluid at a Prescribed Constant Velocity on a Given Streamline.' *Proc. Math. Symp.*, Moscow, Russia, Vol. XV.

LAUBER, G., and HAGER, W.H. (1998). 'Experiments to Dambreak Wave: Horizontal Channel.' *Jl of Hyd. Res.*, IAHR, Vol. 36, No. 3, pp. 291-307.

LEMMIN, U., and LHERMITTE, R. (1999). 'ADV Measurements of Turbulence: can we Improve their Interpretation ? Discussion' *Jl of Hyd. Engrg.*, ASCE, Vol. 125, No. 6, pp. 987-988.

MICHELL, J.H. (1890). 'On the Theory of Free Streamlines.' Phil. Trans. Roy. Soc., London, Part A, Vol. 181, pp.389-431.

MISES, R. von (1917). 'Berechnung von Ausfluss und Uberfallzahlen.' *Z. ver. Deuts. Ing.*, Vol. 61, p. 447 (in German).

MONTES, J.S. (1997). 'Irrotational Flow and Real Fluid Effects Under Planar Sluice Gates.' *Jl of Hyd. Engrg.*, ASCE, Vol. 123, No. 3, pp. 219-232. Discussion: Vol. 125, No. 2, pp. 208-213.

MONTES, J.S. (1998). 'Hydraulics of Open Channel Flow.' *ASCE Press*, New-York, USA, 697 pages.

NIKORA, V.I., and GORING, D.G. (1998). 'ADV Measurements of Turbulence: can we Improve their Interpretation ?' *Jl of Hyd. Engrg.*, ASCE, Vol. 124, No. 6, pp. 630-634. Discusion: Vol. 125, No. 9, pp. 987-988.

NORTEK (1996). '10 MHz ADV Precise Measurements of 3-D Fluid Flow.' Nortek AS, Norway, October.

STORR, G.J., and BEHNIA, M. (1999). 'Experiments with Large Diameter Gravity Driven Impacting Liquid Jets.' *Experiments in Fluids*, Vol. 27, pp. 60-69.

TROSKOLANSKI, A.T. (1960). 'Hydrometry : Theory and Practice of Hydraulic Measurements.' Pergamon Press, Oxford, UK, 684 pages.

VALLENTINE, H.R. (1969). 'Applied Hydrodynamics.' *Butterworths*, London, UK, SI edition.

Notation

A jet cross-section area (m^2); for a rectangular jet, A = B * b;
A tank free-surface area (m^2);
A_o orifice cross-section area (m2);
B free-falling nappe width (m);
b free-falling nappe thickness (m);
B_o orifice width (m) (long dimension);
b_o orifice thickness (m) (small dimension);
$C_{D,}$ orifice discharge coefficient: $C_D=C_C*C_V$;
C_D corrected discharge coefficient;
C_c orifice flow contraction coefficient: $C_C=A/A_O$;
C_v orifice flow velocity coefficient;
g gravity constant (m/s^2);
H total head above orifice (m);
H_1 initial total head above orifice (m);
Q total volume discharge (m^3/s) of water;
q discharge per meter width (m^2/s) : at the orifice $q = Q/B_o$;
t time (s);
t_1, t_2 times (s);
V velocity (m/s);
V_x, V_y, V_z velocity components (m/s) in the x-, y- and z-directions
x horizontal Cartesian co-ordinate (m) along the short orifice dimension; x = 0 at orifice centreline;
y horizontal Cartesian co-ordinate (m) along the orifice width; y = 0 at orifice centreline;
z vertical Cartesian co-ordinate (m) positive upwards; z = 0 at the orifice;

Greek symbols

δ convergence angle into the orifice;
μ water dynamic viscosity (Pa.s);
ν water kinematic viscosity (m^2/s): $\nu=\mu/\rho$;
θ_x lateral spread angle of the bursting flow in the x-direction;
θ_y lateral spread angle of the bursting flow in the y-direction;
ρ water density (kg/m^3);

Subscript

o orifice reference conditions;
x horizontal co-ordinate;
y horizontal co-ordinate;
z vertical co-ordinate;
1 initial flow conditions.

Appendix - discharge coefficients : experimental results

Initial volume m^3 (1)	H_1 m (2)	C_D (3)	C_D' (4)	Comments (5)
0.432	0.314	0.63	0.54	
0.450	0.326	0.64	0.55	
0.439	0.319	0.64	0.55	
0.441	0.321	0.64	0.55	
0.452	0.328	0.64	0.56	
0.492	0.357	0.64	0.56	
0.446	0.324	0.65	0.56	
0.493	0.358	0.64	0.56	
0.435	0.316	0.66	0.57	
0.452	0.328	0.66	0.57	
0.771	0.557	0.63	0.57	
0.774	0.559	0.63	0.57	
0.776	0.560	0.63	0.57	
0.789	0.569	0.63	0.57	
0.791	0.570	0.63	0.58	
0.791	0.571	0.63	0.58	
0.792	0.571	0.63	0.58	
0.793	0.572	0.63	0.58	
0.669	0.484	0.64	0.58	
0.910	0.655	0.62	0.58	
1.03	0.749	0.62	0.58	
1.03	0.751	0.62	0.58	
1.03	0.752	0.62	0.58	
0.702	0.507	0.64	0.58	
0.791	0.571	0.63	0.58	
0.882	0.635	0.63	0.58	
0.883	0.636	0.63	0.58	

Initial volume m^3 (1)	H_1 m (2)	C_D (3)	C_D' (4)	Comments (5)
1.03	0.75	0.62	0.58	
1.03	0.75	0.62	0.58	
1.03	0.752	0.62	0.58	
1.03	0.752	0.62	0.58	
1.04	0.754	0.62	0.58	
1.04	0.754	0.62	0.58	
1.04	0.754	0.62	0.58	
1.04	0.756	0.62	0.58	
1.04	0.758	0.62	0.58	
1.072	0.769	0.62	0.58	
1.074	0.770	0.62	0.58	
0.436	0.317	0.68	0.58	
0.790	0.570	0.64	0.58	
0.887	0.638	0.63	0.58	
0.887	0.638	0.63	0.58	
0.887	0.639	0.63	0.58	
0.888	0.639	0.63	0.58	
0.904	0.651	0.63	0.59	
0.905	0.651	0.63	0.59	
0.905	0.651	0.63	0.59	
0.905	0.652	0.63	0.59	
0.906	0.652	0.63	0.59	
0.909	0.654	0.63	0.59	
0.910	0.655	0.63	0.59	
1.03	0.747	0.63	0.59	
1.03	0.748	0.63	0.59	
1.03	0.75	0.63	0.59	

0.883	0.636	0.63	0.58	
0.885	0.637	0.63	0.58	
0.886	0.638	0.63	0.58	
0.888	0.639	0.63	0.58	
0.904	0.651	0.63	0.58	
0.905	0.651	0.63	0.58	
0.905	0.651	0.63	0.58	
0.906	0.652	0.63	0.58	
0.906	0.652	0.63	0.58	
0.907	0.653	0.63	0.58	
0.908	0.653	0.63	0.58	
0.908	0.653	0.63	0.58	
0.910	0.655	0.63	0.58	
0.910	0.655	0.63	0.58	
1.031	0.740	0.62	0.58	
1.031	0.740	0.62	0.58	
1.031	0.740	0.62	0.58	
1.034	0.742	0.62	0.58	
1.03	0.746	0.62	0.58	
1.03	0.748	0.62	0.58	
1.043	0.748	0.62	0.58	
0.792	0.571	0.74	0.68	Plastic sheets (Fig. 5).
0.441	0.321	0.80	0.69	
0.431	0.313	0.80	0.69	
1.057	0.758	0.76	0.71	
0.441	0.320	0.83	0.71	
0.771	0.557	0.78	0.72	
0.422	0.307	0.84	0.72	
0.440	0.319	0.84	0.73	
1.017	0.730	0.78	0.73	
0.787	0.568	0.80	0.74	

1.03	0.752	0.63	0.59	
1.04	0.754	0.63	0.59	
1.057	0.758	0.63	0.59	
1.05	0.761	0.63	0.59	
0.441	0.320	0.68	0.59	
1.060	0.761	0.63	0.59	
1.076	0.771	0.63	0.59	
0.793	0.572	0.65	0.59	
0.795	0.573	0.65	0.60	
0.774	0.559	0.66	0.60	
1.057	0.758	0.65	0.61	
1.054	0.756	0.66	0.61	
1.075	0.771	0.79	0.74	Plastic sheets (Fig. 5).
0.777	0.561	0.82	0.75	
1.058	0.759	0.81	0.76	
0.788	0.569	0.83	0.76	
0.774	0.559	0.84	0.77	
1.056	0.757	0.82	0.77	
0.772	0.557	0.85	0.78	
0.428	0.311	0.91	0.78	
0.774	0.558	0.88	0.81	
1.055	0.757	0.87	0.81	